Received 5 October 2021; accepted 19 December 2021. Date of publication 28 December 2021;
date of current version 24 January 2022. The review of this article was arranged by Editor Sumei Sun.

Digital Object Identifier 10.1109/OJVT.2021.3138894

A Critical Review of Emerging Technologies for Electric and Hybrid Vehicles

CHRISTOPHER H. T. LEE [1] (Senior Member, IEEE), WEI HUA [2] (Senior Member, IEEE), TENG LONG [3] (Member, IEEE), CHAOQIANG JIANG [4] (Member, IEEE), AND LAKSHMI VARAHA IYER [5] (Senior Member, IEEE)

[1]School of Electrical and Electronic Engineering, Nanyang Technological University, Singapore 639798
[2]School of Electrical Engineering, Southeast University, Nanjing, Jiangsu 211189, China
[3]Department of Engineering, University of Cambridge, CB3 0FA Cambridge, U.K.
[4]Department of Electrical Engineering, City University of Hong Kong, Kowloon, Hong Kong
[5]Department of Electrical Engineering, Magna International Inc., Troy, MI 48098 USA

CORRESPONDING AUTHOR: Christopher H. T. Lee (e-mail: chtlee@ntu.edu.sg)

ABSTRACT Emerging topics such as environmental protection and energy utilization have pushed research and development of electric vehicles and hybrid electric vehicles (EVs/HEVs). In the last few decades, numerous technologies have been developed for EV/HEV importance. In this article, key research topics in the area of EVs/HEVs, namely electric machines, electrochemical energy sources, wireless charging infrastructure, and latest EV/HEV models are covered. This paper aims to consolidate the key emerging technologies in this field and provide the readers a blueprint to begin their own journeys.

INDEX TERMS Electric machine, induction machine, wound field synchronous machine, reluctance machine, stator permanent-magnet machine, field modulation machine, high-speed machine, electrochemical energy source, battery, fuel cell, ultracapacitor, wireless charging infrastructure, part-and-charge, coil design, move-and-charge, electric vehicle, hybrid vehicle.

I. INTRODUCTION

With changing consumer behavior, government regulations and sustainability requirements, research on electromobility applications, in particular electric vehicles and hybrid electric vehicles (EVs/HEVs), has drawn significant attention. It is anticipated that by 2040, annual sale of EVs/HEVs is projected to outsell gasoline and diesel vehicles, with estimated sale over 48 million per year. As one of the most promising electromobility applications, the development of EVs/HEVs has become a hot research topic.

This paper aims to provide a critical review of emerging technologies for EV/HEV applications. It aims to cover key research topics, including electric machines, electrochemical energy sources, wireless charging infrastructure and latest EV/HEV models. The purpose of this paper is to provide potential readers, including engineers, researchers and scholars, a critical review of latest technologies in area of EV/HEV applications.

II. ELECTRIC MACHINES

Due to the definite merits of high efficiency, high power and torque densities, permanent-magnet (PM) machine has served as a promising candidate for EVs/HEVs. Meanwhile, other types of machines, e.g., induction machine (IM), would field synchronous machine (WFSM) and reluctance machine, have also gained attention for automotive applications in the past 20 years. For example, IMs have been employed in Tesla EVs and wound-rotor synchronous machines in Renault Zoe EV and BMW iX3 e-Drive.

A. INDUCTION MACHINES (IMS)

PM machines have been widely applied in many applications due to its high torque density and efficiency. However, PM machines suffer from some disadvantages, e.g., unstable rare-earth supply, low flux-weakening capability and irreversible demagnetization. Therefore, global efforts are underway in developing non-PM machines, among which the IM is the most successful type for EV/HEV applications.

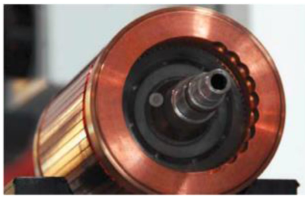

FIGURE 1. The copper rotor of IM used in Tesla Model S [7].

Being an AC machine, an IM exhibits two windings separated by an air-gap [1], [2], where all electromagnetic energy is transferred by inductive coupling from the primary winding to the secondary winding. The IM-based drives offer the advantages of robust structure, low cost, high reliability, and maintenance-free [3]. Therefore, the squirrel-cage IMs are widely employed in EVs/HEVs for high torque/power density, high efficiency, strong physical structure, and variable speed range [4]. However, most IMs have lower efficiency and less torque density than PM machines [5]. To address this situation, an IM with copper rotor cage is utilized for the driving system of Tesla EVs to improve the torque density and efficiency, as shown in Fig. 1 [6], [7]. Besides, the innovative rotor manufacturing called as short-circuit ring and connection with the copper rod is proposed by Siemens [8]. With optimized material and suitable cooling technique, the power density and efficiency of the IM can be almost the same as with synchronous motors [9]. In addition, an axial-flux IM, with double-sided axial fluxes, is also an attractive solution. This structure can significantly increase torque density and has the potential to become a compact and cost-effective machine [10], [11]. Another high efficiency IM with compact stator winding form, which allows modifying overhang deviation and ruling thermal condition, is proposed in [12]. Apart from developing the structures with improved torque density, a novel control method in the feedback channel based on morphological filters is proposed to suppress torque ripple by current harmonics [13].

Apart from the squirrel-cage IMs, the doubly-fed IM (DFIM) has also proved to be a competitive candidate for EVs/HEVs with the improved efficiency and extended torque-speed characteristics compared to its singly-fed counterpart. A dual-electrical-port control scheme of cascaded brushless doubly-fed IM (CBDFIM) is proposed to achieve doubled constant torque and constant power regions compared to its singly-fed counterpart with the same equivalent pole pair number [14]. Another single-electrical-port control scheme for four-quadrant operation of cascaded doubly-fed IM (CDFIM) is proposed and theoretically demonstrated. It is found that the doubly-fed synchronous operation of the CDFIM can achieve a wider constant torque region and constant power region than the singly-fed synchronous operation [15].

B. WOUND FIELD SYNCHRONOUS MACHINES (WFSMS)

For EV/HEV applications, another successful machine type is the wound rotor synchronous machine (WRSM) [16], as

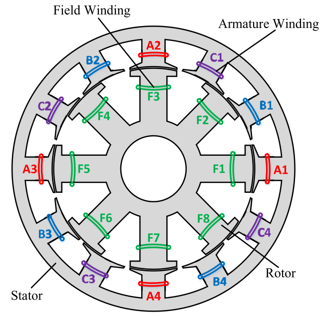

FIGURE 2. Topology of wound rotor synchronous machine [16].

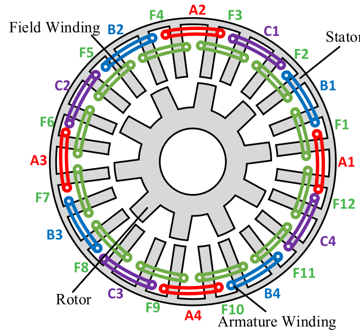

FIGURE 3. Topology of wound field switched flux machine [17].

depicted in Fig. 2. To remove brush and ring in WRSMs, the wound field switched flux machine (WFSFM) is proposed [17], [18], as depicted in Fig. 3. The above two machines both belong to the family of WFSMs with wound field winding in rotor and stator, respectively.

The conventional WRSMs are widely applied as low-speed generators [19]–[22], while the rotor field winding excitation system has a large volume and low power density. Therefore, the brushless operations of WRSMs are studied with various topologies [23]–[27].

WFSFMs have both armature and field windings on stator, which realize brushless operation [28], [29]. According to the winding arrangements, it can be divided into three types, namely, the one with both armature and field coils wound on one tooth [17], the one with half tooth wound by armature coils and the other by field coils [30], and the one with overlapped armature and field coils [29]. According to iron steel topology, it can be further divided as single stator [28]–[30] and double-stator [31]. It should be noted the latter one has a higher slot area and higher slot packing factor, and hence potentially higher torque/power density.

Recently, field winding induced voltage due to the harmonic flux linkage in WFSMs have received considerable attention [32]–[38]. However, these machine types suffer from deteriorated control performance and risks of damaging the field winding power supply. To cope with these problems, various reduction methods, including skewing [32], [33], chamfering [34], axial pairing [34], stator damper winding [37],

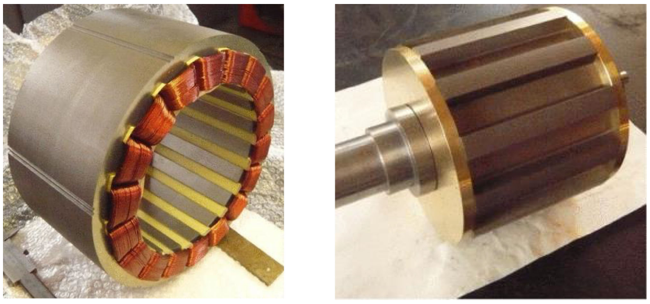

(a) (b)

FIGURE 4. Stator and rotor of the prototype SRM [44].

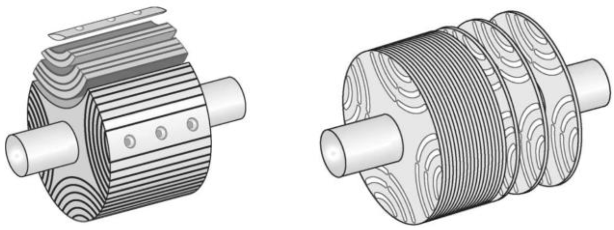

(a) (b)

FIGURE 5. Rotor topologies of SynRMs [48]. (a) AL rotor. (b) MB rotor.

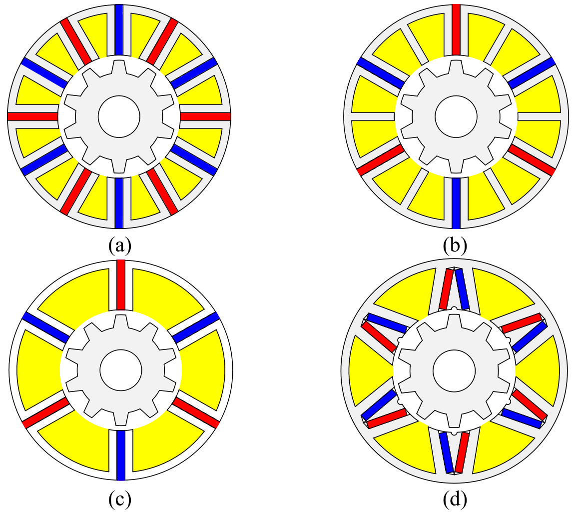

FIGURE 6. Various FSPM machines for EV/HEV applications. (a) U-shaped [56]. (b) E-shaped [57]. (c) C-shaped [58]. (d) V-shaped [59].

are proposed. The mechanism and modeling of field winding induced voltage in WFSMs are shown in [32], [34], [38].

C. RELUCTANCE MACHINES

Switched reluctance machines (SRMs) have attracted significant attention due to their inherent advantages, such as simplicity, robustness, excellent fault-tolerance, and wide speed range. During the last few decades, as a PM-free brushless machine, the SRM-based drive systems have accelerated developments due to the supply limitation and price fluctuation of rare-earth materials [39]. Hence, SRMs are considered as strong candidates for EVs/HEVs.

In 1998, a 300Nm SRM with outer diameter/axial length of 296mm/ 96mm was reported, where the torque density of 38Nm/L was achieved in experiments though the current density as 50A/mm^2 [40]. In 2008, the SRM for mild HEVs with outer diameter/axial length of 410mm/93mm was built with the electromagnetic torque of 300Nm. It could provide the torque density of 25Nm/L and the highest efficiency of 96% [41]. In 2010, the SRM with electromagnetic torque of 1800Nm, torque density of 30Nm/L was reported with outer diameter/axial length of 640mm/190mm [42].

Tokyo University of Science compared the electromagnetic performance of SRMs with 12/8 and 18/12 structures, from the point of view of torque density, efficiency, and torque-speed range. It was found that the performance of 18/12 machine is better [43]. In [44], a 50-kW prototype SRM was built and comprehensively tested as shown in Fig. 4 . The maximum efficiency, output power, and torque density reached 95.4%, 54.1kW, and 38Nm/L, respectively. These values were competitive to the IPM motor employed in Toyota Prius 2003 (i.e., an HEV).

Although SRMs with comparable torque/power density to the IPM motors are reported, no single electrified passenger vehicle with an SRM exists in market [45]–[47] due to noise, vibration, torque ripple, and unique inverter, which indicates that the SRMs need further development.

Synchronous reluctance machine (SynRM) can be regarded as a potential candidate for alternative of PM machines in EVs/HEVs due to low cost and environmentally friendly. Different from SRMs, rotors of SynRMs are relatively complicated [48], which can be divided as axially laminated (AL) rotor [49], [50] and multi barriers (MB) [51]–[54] rotor, as shown in Fig. 5.

SynRM with AL rotor has higher saliency ratio that can help achieve higher torque density. However, AL rotor suffers from high manufacturing difficulty and fragile structure, which limit its application. Although the saliency ratio is reduced, MB rotor is more robust and simpler. Therefore, MB rotor receives considerable attention in recent years. In general, SynRM suffers from drawbacks as complicated rotor structure, non-linear characteristic and high torque ripple. The optimization of machine topology is studied in [50], [51], and the effect of saturation is considered in [52], [53]. The acoustics issue by torque ripple is optimized in [54]. In short, SynRM consists of some inherent problems and its application in EVs/HEVs is still in the developing stage.

D. STATOR-PM MACHINES

As a topology of novel brushless PM machines, stator-PM machines having magnets and armature windings on its stator (the so-called as stator-PM machines), exhibit the merit of convenient heat dissipations [55]. The compact and robust rotor structure also makes stator-PM machines as potential candidates for high-speed applications. Meanwhile, the air-gap flux regulations can be realized by hybrid excitations of PMs and field windings. In general, stator-PM machine features the definite advantages of robust structure, high power density and efficiency, high fault-tolerant capability. These advantages allow stator-PM motors to be a suitable candidate for EVs/HEVs.

Generally speaking, the flux-switching PM (FSPM) machine attracts more attention since it exhibits largest torque/power density within the stator-PM machine family. The most typical structure was proposed by E. Hoang in 1997, as shown in Fig. 6(a) [56], where its stator consists of 12 "U-shaped" silicon steel and 12 magnets. In order to reduce the PM usage, a new E-shaped structure is proposed [57], as shown in Fig. 6(b). It is found that the improved topology can reduce the PM usage by half while the torque remains almost the same. However, this topology suffers from poor overload capability. In order to further increase the slot area, another C-shaped structure is proposed in [58], as shown in Fig. 6(c). Similarly, the amount of PM is half as compared to that of traditional FSPM machine. To further improve the torque and PM utilization, a V-shaped structure is proposed in [59], as shown in Fig. 6(d). Compared with the traditional topology, a pair of magnets with opposite magnetizing directions are placed on each stator tooth, and the two magnets can therefore form a V-shaped structure. To further improve the utilization of PMs, a FSPM machine with a multi-tooth structure based on the above-mentioned V-shaped structure is proposed in [60]. To expand the speed adjustment regions, the air-gap flux regulations can be realized by hybrid excitations of PMs and field windings [61]–[67].

E. FIELD MODULATION MACHINES

Field modulation machine (FMM) is a general designation for a class of machines with modulation effect. FMMs include stator-PM machines and PM vernier (PMV) machines [68]–[71]. In general, FMMs utilize magnetic flux modulator to modulate the speed and pole-pair numbers of the initial magnetic field [72], [73]. Most of the air-gap magnetic field harmonics in FMMs can contribute to torque, and hence an improved torque density can be achieved [74]. According to air-gap field modulation theory [75], [76], the pole-pair of air-gap magnetic field harmonics in field modulation machines can be expressed as

$$p_h = |mp \pm in_s| \tag{1}$$

where p indicates the pole-pair of the magnetic field due to PM or armature windings, n_s expresses the pole-pair of the magnetic flux modulator, m and i are the modulation coefficients.

The PM layouts of stator-PM machines are usually fixed [77], [78]. Meanwhile, the PMV machines consist of a more flexible PM layout, where PMs can be mounted on rotor, on stator teeth, stator yoke, and both stator and rotor [79]–[82], as shown in Fig.

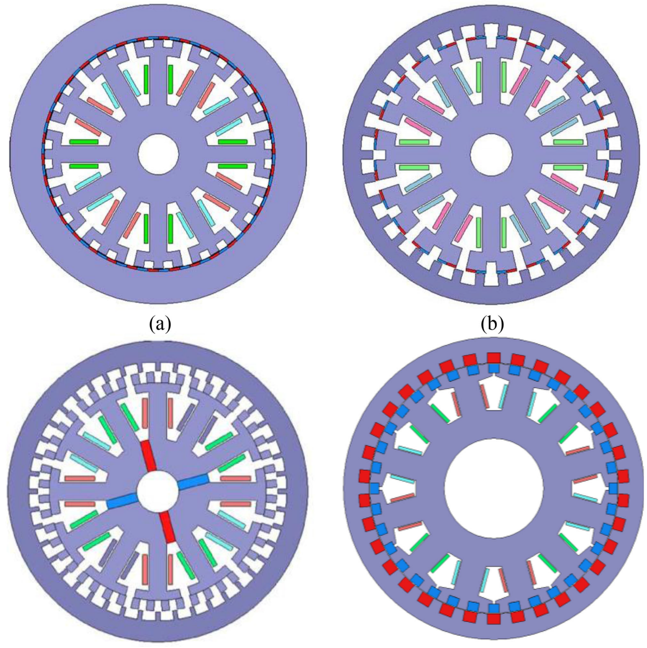

FIGURE 7. PMV machines with different PM layouts [79]–[82]. (a) On the rotor. (b) On the stator teeth. (c) In the stator yoke. (d) On both the stator and rotor.

In [81], it is confirmed that the PMV machines in Fig. 7(a) can offer a higher no-load EMF and torque handling capability. S. L. Ho pointed out that the performances of PMV machines with PMs on the rotor in Fig. 7(a) are better than those with PMs on the stator teeth in Fig. 7(b) or in the stator yoke in Fig. 7(c) [82]. S. Shimomura found that the PMV machine with multi-slot on the stator teeth [see Fig. 7(d)] can reduce the armature current and loss to improve efficiency [80]. In addition, by changing the rotor PMs from surface mounted to spoke array, the torque and power density of the PMV machine can be further improved [83].

F. HIGH-SPEED MACHINES

EV/HEV machines should not only satisfy specific requirements in performance and efficiency, but also noise, vibration and harshness, cost [84], [85]. With the rapid development of traffic electrifications, high-speed machine has attracted more and more attention. This type of machines has been applied in the automotive industry because of its characteristics of high power density, high efficiency, lightweight and low cost. The main types of high-speed machines used in vehicle drive, supercharger and vehicle compression include PM synchronous machine (PMSM), IM, SRM, and SynRM. In recent years, PMSM has outstanding advantages in power density, torque density, efficiency and speed regulation range and is widely used in EVs/ HEVs [86], [87]. For example, commercially available Honda, Toyota, Tesla and BMW vehicles use PMSM as its propulsion motor. The disadvantage of PMSM comes from the fact that it adopts rare earth PM, which has a high

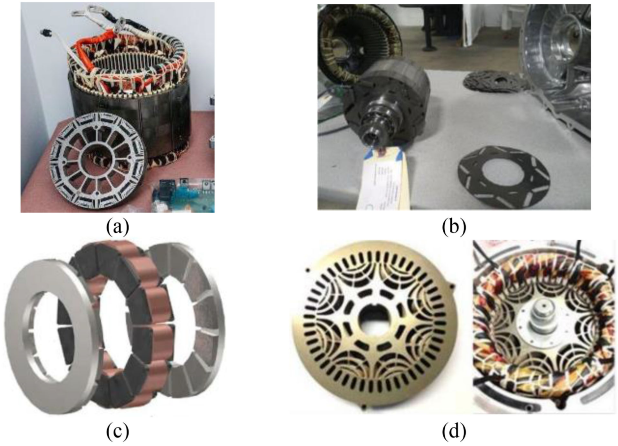

FIGURE 8. High-speed machines in the market. (a) BMW i3 [95]. (b) Tesla Model 3 [87]. (c) YASA-400 [96]. (d) GM ELT093 [97].

cost and risk of thermal demagnetization. IM has no magnets in the rotor and is characterized by its robustness. The limitation of this topology may lie in the cooling system, where heat is generated on the rotor and stator sides. SRM does not rely on PMs and is very robust for harsh environments and fault-tolerant operation [88]. However, SRMs suffer from high noise and low power factors [89], [90]. SynRM has been studied more recently [86], [91], [92]. By using the reluctance torque, the amount of PM so as the cost are reduced, but SynRM still suffers from serious problems of rotor deformation and magnetic flux leakage during high-speed operation [93], [94].

Many automobile companies have studied the high-speed machines and formed a series of products. The high-speed machine of BWM i3 pure EV is a PMSM, which consists of maximum power 125kW, peak torque 250Nm, maximum speed 11400rpm, and mass 42kg [95], as shown in Fig. 8(a). The Tesla Model 3 uses a 6-pole 54-slot PMSM with a maximum speed of 18,000rpm and a maximum power of 196kW. This PMSM consists currently the highest speed on the market [87], as shown in Fig. 8(b). Oxford University uses axial flux PM machines, which leads to a series of produce line, such as YASA-400 and YASA-750. Taking YASA-400 as an example, it consists of the maximum speed 7500rpm, and the maximum power 165kW [96], as shown in Fig. 8(c). General Motors (GM) has launched an advanced automotive technology project codenamed ELT093 [97]. Its SynRMs can provide rotation speed 16650rpm, and the torque 250Nm, as in Fig. 8(d).

Z. Yang [84] presented the design and comparative evaluation for PMSM, IM, and SRM for EV/HEV applications. Simulation and analytical results show that each machine topology demonstrates its own unique characteristic. IM and SRM have lower peak power density, i.e., 50kW/48kg and 50kW/42kg respectively, comparing with 50kW/30kg for PMSM. The PMSM, IM and SRM for a supercharger application operating for a short duty only at a constant speed were compared in detail [98]. A comparison between the PMSM and SPM machines is carried out for application to an EV, in terms of performance at given inverter ratings [99].

III. ELECTROCHEMICAL ENERGY SOURCES

Electrochemical energy source can be used to power not only electric motor drives, but also other auxiliary parts, such as air conditioners, lightings, audiovisual systems within the EVs/HEVs. Existing electrochemical energy sources are able to provide either high specific energy or high specific power (or also known as energy density and power density), but not at the same time. There are plenty of electrochemical energy sources available in the market, while they can be roughly categorized into three key groups, namely batteries, fuel cells and ultracapacitors.

A. BATTERIES

Battery is an electrochemical conversion device that can convert between active materials and electric energy [100]. It typically contains three key parts, namely positive electrode, negative electrode and electrolyte. Depending on different applications, many various types of batteries have been developed in last few centuries. For EV/HEV applications, there are mainly three major types of candidates, namely lead-acid battery, nickel-based batteries and lithium-based batteries [101].

Lead-acid battery is widely regarded as one of the first commercially available battery in EV/HEV applications. Typical lead-acid battery employs lead dioxide as positive electrode and metallic lead as negative electrode. Unlike conventional lead-acid battery, an improved lead-acid battery, so-called as value regulated lead-acid (VRLA) battery, consists of electrolyte of two forms, namely absorbed electrolyte and gelled electrolyte. These two-formed structure allows VRLA battery to reduce evaporation, leakage and vibration, as compared to its conventional counterparts. Even conventional lead-acid and VRLA batteries consists of different topologies, both share the same chemical reactions as:

$$Pb + PbO_2 + 2H_2SO_4 \leftrightarrow 2PbSO_4 + 2H_2O \tag{2}$$

The first nickel-based battery was invented more than a century ago and this type of battery has been widely employed in many applications, including EVs/HEVs. There are plenty types of nickel-based batteries, such as nickel-iron (Ni-Fe), nickel-cadmium (Ni-Cd), nickel-zinc (Ni-Zn) and nickel-metal-hydride (Ni-MH) batteries, while the most common one in EVs/HEVs is Ni-MH battery. Similar as other nickel-based batteries, Ni-MH battery employs nickel hydroxide as its positive electrode. Meanwhile, it employs metal hydride as negative electrode and potassium hydroxide solution as electrolyte. There are various types of metal hydride available, while the most common one is AB_2 alloy and AB_5 alloy. The typical chemical reaction of Ni-MH battery can be described as:

$$MH + NiOOH \leftrightarrow M + Ni(OH)_2 \tag{3}$$

TABLE 1. Comparisons of Typical Batteries

	Lead-acid	Nickel-based	Lithium-based
Specific energy (Wh/kg)	30 – 50	30 – 75	120 – 180
Specific power (W/kg)	150 – 200	150 – 450	200 – 400
Cycle life (Cycle)	400 – 800	800 – 2000	600 – 1200

Lithium battery employs various types of materials as its positive electrode while lithium metal as its negative electrode, as how it is named. However, lithium metal leads safety problems, including storage, transportation and operation. Hence, to improve the situations, intercalation material is used to replace lithium metal as its negative electrode, and hence forming the lithium-ion (Li-ion) battery. Typical Li-ion battery employ lithium intercalation compounds as both its positive and negative electrodes. During charging and recharging processes, lithium ions are inserted and removed between positive and negative electrodes. In principle, there is no net change during movement of lithium ions. Depending on various type of employed materials, chemical reaction of Li-ion battery can be described as:

$$LiYO_2 + C \leftrightarrow Li_xC + Li_{1-x}YO_2 \tag{4}$$

To evaluate performances of batteries, three major key index, namely specific energy, specific power and cycle life, are usually used. Specific energy is the energy capacity available with a battery while specific power is the energy delivered by a battery within a particular period. Cycle life is the number of maximum charging and recharging cycle of a battery can undergo without significant again effect. The comparisons between typical batteries are listed in Table 1.

B. FULL CELLS

Full cell is an electrochemical energy sources that can convert chemical energy into electrical energy [102]. Full cell shares both similarity and dissimilarity as battery does. For the similarity, both two devices share similar structure and hence consume fuels and oxidants to perform chemical reactions. For the dissimilarity, the battery stores the fuel and oxidants within the system while the fuel cell stores these materials outside the system. For EV/HEV applications, there are four promising candidates, namely alkaline fuel cell (AFC), phosphoric acid fuel cell (PAFC), proton exchange membrane fuel (PEMFC) and direct methanol fuel cell (DMFC).

AFC has been generally accepted as the first practical fuel cell while it was firstly proposed by Sir William Robert Grove in 1800s. Typical AFC operates with pure hydrogen, pure oxygen and circulating electrolyte. It enjoys definitely merits of high efficiency, mature technology and cost-effectiveness. It contains two porous electrodes, separated by matrix saturated alkaline solution. Before of efficient heat transfer rate, potassium hydroxide (KOH) is widely commonly employed in AFC. AFC is operated under redox reaction, i.e., reduction-oxidation reaction as:

$$CO_2 + 2KOH \rightarrow K_2CO_3 + H_2O \tag{5}$$

TABLE 2. Comparisons of Typical Fuel Cells

	AFC	PAFC	PEMFC	DMFC
Common fuel	H_2	H_2	H_2	Methanol
Power density (W/m^3)	1000 – 3000	800 – 2500	3500 – 6500	1500 – 3500
Temperature (°C)	50 – 150	150 – 220	50 – 100	< 100
Efficiency (%)	40 – 60	40 – 55	45 – 60	30 – 40

PAFC is one of the most mature technologies among all fuel cells and it has been widely regarded as the first commercialized fuel cell in electric power industry. It utilizes liquid phosphoric acid as its electrolyte while platinum-coated carbon as catalyst. Electrons can move from negative electrode to positive electrode via external circuit, while positively-charged hydrogen ions is able to transfer from positive electrode to negative electrode via acidic electrolyte. Since PAFC needs to operate in a relatively higher temperature range, phosphoric acid is usually employed as electrolyte. When PAFC generates electricity, it produces water as by-product as:

$$H_2 + \frac{1}{2}O_2 \rightarrow H_2O \tag{6}$$

PEMFC employs proton conducting membrane in solid polymer form as electrolyte, while sometimes it is also called as ion exchange membrane fuel cell or solid polymer electrolyte fuel cell. PEMFC is renowned its high power density and it was the first fuel cell that employed in NASA's Gemini space project in 1960s [103]. To improve stability and lifetime of membrane, operating temperature of this type of fuel cell is usually kept low. Since its operating temperature is relatively low, as compared with other fuel cells, it needs expensive platinum metal as catalyst for chemical reactions. When PEMFC generates electricity, it produces water as similar as PAFC does.

Unlike other fuel cells that employ hydrogen as major fuel, DMFC instead utilizes methanol as its direct fuel. As compared with using hydrogen, using methanol enjoys simpler storage and more compact system. By using methanol as its direct fuel, DMFC can generate electric energy based on electrochemical reactions. Meanwhile, methanol can be firstly transformed as hydrogen reformate gas mixture and stored within the fuel cell and this system is known as indirect methanol fuel cell (IMFC). IMFC behaves similarly as other fuel cell do, which all of them uses hydrogen as its major fuel. Depending on design of DMFC, it can produce carbon dioxide and water as:

$$CH_3OH + \frac{3}{2}O_2 \rightarrow CO_2 + 2H_2O \tag{7}$$

To evaluate performances of fuel cells, four major key index, namely common fuel, power density, temperature and efficiency, are used. Power density is the total power generated by a full cell per unit of volume, while temperature is operating temperature. The comparisons between typical full cells are listed in Table 2.

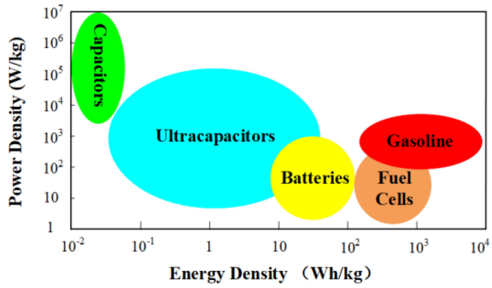

FIGURE 9. Comparisons among various energy sources for EVs/HEVs.

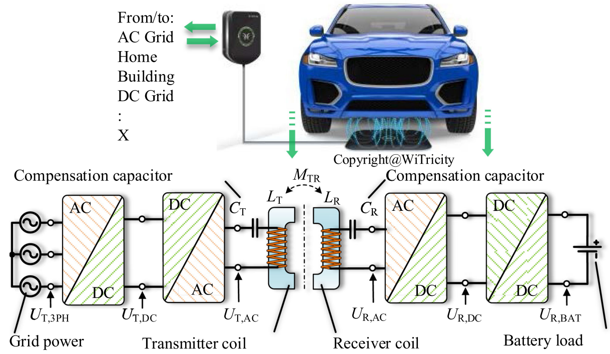

FIGURE 10. Typical configuration for park-and-charge IPT system.

C. ULTRACAPACITORS

Capacitor is a simple device with two metallic electrodes separating by dielectric, while it can store and release electrons in different occasions [104]. Classical capacitors can be grouped into two major types, namely electrostatics capacitor and electrolytic capacitor. The former one uses non-electrolytic materials to act as dielectric component, while the latter one uses electrolytic materials to act as dielectric component. Even though the electrolytic capacitor consists of higher capacitance than the electrostatics one, both of them are still far from sufficient capacity for EV/HEV applications. While capacitors have suffered from low capacity for many years, a new technology known as ultracapacitor has been invented to become a promising solution. There are typically two major types of ultracapacitors available, namely double layer capacitor and pseudocapacitor.

The concept of double layer capacitor allows the charge to be stored on the electrode surface with separated electrode and electrolyte [105]. This idea was not very popular before the technology breakthrough of nanotechnology. Upon support of the latest nanotechnology, capacitor electrodes can be developed based on highly porous materials. This new material characteristic allows the double layer capacitor to become highly capacitance. It should be noted the operating principle of double layer capacitor is generally regarded as a non-Faradic process, i.e., no chemical reaction is associated with charging/discharging process.

Pseudocapacitor is another ultracapacitor with similar idea and topology of double layer capacitor. Pseudocapacitor differentiates itself by oxidation-reduction reactions at its interface and Faradic process, i.e., chemical reaction is associated with charging/discharging process. Since Faradic process is involved within pseudocapacitor, it generally can offer higher capacitance and higher energy density than double layer capacitor.

Comparisons among four major electrochemical energy sources, namely batteries, fuel cells, capacitors and ultracapacitors, and gasoline are shown in Fig. 9.

IV. WIRELESS CHARGING INFRASTRUCTURES

Aiming to mitigate the manual charging with user interaction and eliminate the galvanic connection, the wireless power transfer (WPT) technique offers an unobtrusive and hassle-free charging method regardless of the harsh environment [106]–[108]. In addition, no need to mechanically move charging cable will particularly promote automatic wireless charging technology, and then be more attractive for public transportation with opportunity wireless charging. Among several coupling mechanisms for WPT techniques such as inductive coupling, capacitive coupling, magnetodynamic coupling, and microwaves, as listed in Table 3, the magnetic-resonant coupling (MRC) based inductive power transfer (IPT) has been recognized as the most feasible and the most commonly applied for wireless EV charging application [109]–[111].

A. PARK-AND-CHARGE OF STATIONARY CHARGING

In order to facilitate the park-and-charge (PAC) process for the EVs, the IPT technology is extended to be plug-less, in which the primary coil is installed on the floor of a garage or in a parking lot and the secondary coil is installed on the vehicle, as shown in Fig. 10. The driver needs no bothering about those cumbersome and dangerous charging cables. The use of this system is very easy and the charging process takes place automatically once the driver parks the EV correctly [112]–[114]. This plug-less PAC not only increases user convenience, but also offers a means of overcoming the standardization of charging plugs. Based on magnetic resonant coupling, the primary and secondary coils having the same resonant frequency can wirelessly transfer power efficiently with high power density, while dissipating relatively little energy in non-resonant objects such as vehicle bodies or drivers.

The latest research and development of WPT for PAC are active and diversified, such as compensating the misalignment between magnetic couplers, realizing bidirectional WPT between chargers and EVs, integrating power transfer and information transfer within the same channel. Some state-of-the-art works are summarized below:

1) For realistic PAC, the magnetic coupler design plays a key role for effective WPT. For instance, the compound primary pad using uneven pitch distances of the spiral winding has been proposed to offer a uniform magnetic flux density at most of the charging area, hence solving the problem of misalignment. Meanwhile, the bipolar

TABLE 3. Classification of WPT Technologies for Wireless EV Charging

Energy-carrying medium	Technology		Power	Range	Efficiency	Comments
Electromagnetic field	Near field	Traditional IPT	High	Low	High	Range is too small for EV charging.
		MRC IPT	High	Medium	High	Capable for EV charging.
	Far field	Laser or microwave	High	High	Low	Need direct line-of-sight transmission path, large antennas, and complex tracking mechanisms.
		Radio wave	High	High	Low	Efficiency is too low for EV charging.
Electric field	Capacitive power transfer		Low	Medium	High	Both power and range are too small for EV charging.
Mechanical force	Permanent magnet coupling - Magnetic gear		High	Medium	Medium	Capable for EV charging.

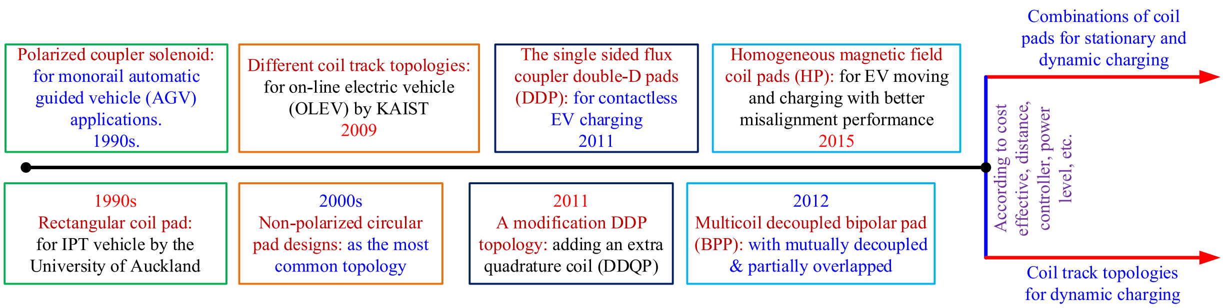

FIGURE 11. Development of WPT typical coil topologies.

primary pad has been developed, which can interoperate with simple secondary pads to achieve power transfer with large lateral tolerance [115].

2) Since EVs can serve as mobile power plants to support and stabilize the power grid with renewables, the development of vehicle-to-grid (V2G) technology is promising [116]. By incorporating the WPT into the V2G, a bidirectional power interface has been developed to facilitate the simultaneous charging and discharging of multiple EVs. Various bidirectional resonant inverters have recently been developed for wireless V2G, aiming to improve the power level, power flow control and fault-tolerant ability [117].
3) The simultaneous wireless power and information transfer (WPIT) technology is being actively developed for EV charging, which desires power transfer from the charger to the vehicle and data communication between the charger and on-board battery management system. A WPIT system has been proposed in which the fundamental component of the triangular current waveform is employed to transfer power, and its third-order harmonic component is selected to transfer information [118].

B. COIL DESIGN OF WIRELESS EV CHARGING

The development of WPT typical coil technologies is depict in Fig. 11. As the energy carrier in WPT system, the transmitter and receiver pads play an important role in emitting and

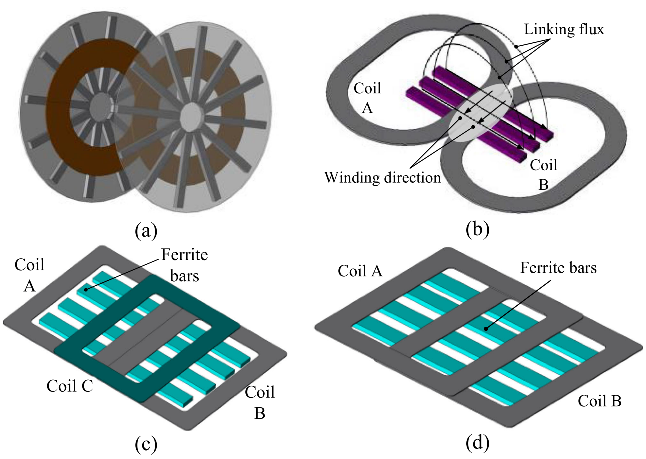

FIGURE 12. Different coil pads for wireless EV charging. (a) Typical single-coil non-polarized circular pad (CP). (b) Polarized double-D pad (DDP). (c) Multiple-coil polarized double-D quadrature pad (DDQP). (d) Multiple-coil polarized bipolar pad (BPP).

receiving the magnetic flux lines. The typical coil topologies for the transmitting coil design and the receiving coil design are shown in Fig. 12, which can be used at the EV side for both park-and-charge and move-and-charge. In the early development of WPT, the rectangular pad was proposed for many years, which consists of four fillets [119]. This topology mainly improves the flux area; and the flux leakage in the edge can be reduced. However, the low efficiency and the large total

TABLE 4. Comparison of Commonly Used Coil Pads with Factors and Features

	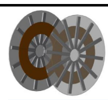	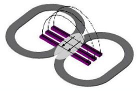	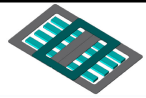	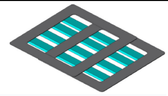
Type	**CP**	**DDP**	**DDQP**	**BPP**
Factors	• Limited cost and size. • System weight. • Types of electric vehicle. • Power level. • Distance between the primary and secondary. • Chassis structure.	• Length and thick of ferrite bars. • Unwanted flux leakage. • Limited system cost and size. • System weight. • Power level. • Requirement of coupled flux direction.	• Length and thick of ferrite bars. • Control methods. • Limited system cost and size. • System weight. • Types of electric vehicle. • Power level. • Chassis structure.	• Length and thick of ferrite bars. • Limited system cost and size. • Overlap of the central area. • Power level. • Distance between the primary and secondary. • Chassis structure.
Features	• Flux symmetric around CP center. • Nonpolarized perpendicular field pattern by CP. • Most commonly used in the primary or secondary. • Poor interoperability characteristics. • Generate and couple perpendicular flux. • Flexible applications.	• Single sided flux generation. • Perform better and be interoperable with different secondary topologies. • Commonly used in the primary. • Ferrite bars easy to be saturation at high power rate. • No reverse flux to eliminate the unwanted rear flux.	• As a secondary, providing z charge zone three times than DDP. • Perform better with different secondary topologies. • Commonly used in the secondary. • Variable excitation modes • Inferior material usage efficiency. • Versatile in central coil design to fit the airgap.	• Mutually decoupled partially overlapped coil structure. • Almost the same performance of DDQP used as a secondary. • Using less copper than DDQP. • Perform better with different secondary topologies. • Commonly used in the secondary. • Almost identical power with DDQ for given size.

flux leakage are indispensable. Thus, it is normally accepted for the transmitting coil design according to the specific requirement. In order to facilitate a low reluctant flux path and reduce the flux leakage, ferrite bars are presented to add to the back of the coil pad, as shown in Fig. 12(a). Also, an aluminum plate is created at the back of the whole coil to hold up the flux distribution. This topology takes the advantage that the structure is easy to build with the symmetric flux distribution around the center. However, the transfer distance, namely the main flux height, is limited by the pad size.

Based on the CP topology, an improved topology called DDP, as shown in Fig. 12(b), was proposed, where the currents in double coils are in opposite direction. The flux path can be created to narrower and taller due to the parallel field pattern along the ferrite bars [120]. Hence, the transmission distance can be extended with high efficiency. However, this topology behaves poor interoperability characteristic when the receiver pad is centrally aligned, as well as the CP topology. To overcome this interoperability problem, the DDQP topology was design to generate both parallel and perpendicular magnetic field [121]. The DDQP topology was placed one additional coil on DDP topology, which is shown in Fig. 12(c). Since the DDQP topology can generate the polarized and non-polarized field by regulating the coil current, the system flexibility is higher than other topologies. But the drawback is the increased number of coils, which leads to the increased cost.

Comparing to the DDQP topology, another high flexibility topology called BPP was introduced to generate the parallel and perpendicular filed, where the two coils are partially overlapped, as shown in Fig. 12(d). In the meantime, the system complexity and cost are reduced by eliminating one coil. According to the different operations of the current direction, the BPP topology can work in CRP mode, single coil mode, and DD mode. Hence, the BPP topology can be effectively suitable for multi-mode secondary pad design, which has a big potential for wireless EV charging [122]. In addition, the comparison of commonly used coil pads with factors and features is summarized and listed in Table 4.

C. MOVE-AND-CHARGE OF DYNAMIC CHARGING

Rather than stopping or parking, the EV prefers to be wirelessly charged during moving. Namely, an array of power transmitters is embedded beneath the roadway (so-called the charging zone or lane) while a receiver is mounted at the bottom of the EV. This move-and-charge (MAC) technology has high potentiality to fundamentally solve the long-term problems of the EV. Namely, there is no need to install so many batteries in the EV, hence dramatically cutting its initial cost; and the EV can be conveniently charged at the charging zone during driving, hence automatically extending the driving range. Differing from PAC, the system configuration for MAC is more challenging.

The transmitters installed beneath the road surface can be either pad or rail design. The pad design includes many primary pads where the size of each pad is equal to or less than that of a vehicle. Based on one power inverter per section, the primary pads can be separately excited by using power switches and sensors as shown in Fig. 13(a). These pad-based transmitters inevitably involve a large amount of primary pads, power inverters or power switches and sensors, thus suffering from huge investment costs and high installation complexity. In contrast, the rail design involves only a primary rail or actually a long primary coil and a power inverter to feed multiple EVs, as shown in Fig. 13(b), which takes the definite advantage of much lower investment cost and much lower installation complexity than the pad design. For the sake of more flexible maintainability and scalability, the rail design usually adopts the arrangement of sectionalized roadway in

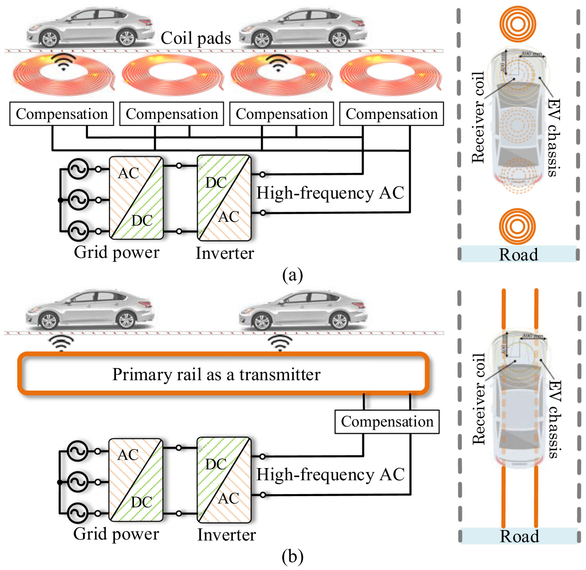

FIGURE 13. Coil configuration of the move-and-charge system. (a) Multiple coil pads as the primary transmitter. (b) Single coil rail as the primary transmitter.

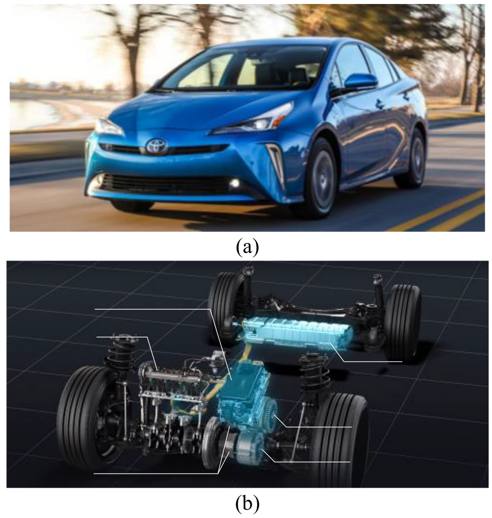

FIGURE 14. Toyota Prius XLE AWD-e [130]. (a) Overall view. (b) Hybrid transaxle.

which it uses one power inverter per section to feed multiple EVs.

Because of the potentiality to fundamentally solve the long-term problems of EVs, research and development of MAC technology have been overwhelming. Some state-of-the-art works for MAC are summarized below:

1) The online electric vehicle (OLEV) project conducted by KAIST has successfully implemented the rail-based MAC system. It has solved various MAC problems such as high-frequency current-controlled inverters, continuous power transfers, and cost-effective improvement. Innovative coil designs and roadway construction techniques make the system efficiency of the OLEV reach up to 83% at an output power of 60 kW with a resonant frequency of 20 kHz. Different magnetic couplers using a rail have been well developed for the move-and-charge system, such as the U-type, E-type, W-type, I-type, and S-type rails [123]–[125].
2) Due to the mobility of the EV, the misalignment between the primary and secondary coils of the pad-based MAC system inevitably affects the performance of existing WPT techniques. The homogeneous WPT technique has been proposed [126], [127], which utilizes the alternate winding design to gaplessly assemble primary coils to enhance the magnetic flux density, and the vertical-and-horizontal secondary coil to improve the capability of acquiring energy, especially in the area of the coils gap. Hence, it can effectively improve the power transfer performance of this pad-based MAC system.
3) In order to allow authorized EVs to perform charging and avoid unauthorized EVs stealing wireless power when they are running on the rail-based MAC system, the energy encryption technique has been proposed [128]. Namely, the operating frequency is purposely adjusted to follow a predefined sequence over a predefined frequency band (so-called the security key) while the primary rail is synchronously tuned to have the resonant frequency matching with the operating frequency, the transmitted energy is thus encrypted. When the secondary coil is also synchronously tuned to have the same resonant frequency in accordance with the security key, the authorized EV can receive the desired energy; otherwise, without the knowledge of the security key, the unauthorized EV cannot decrypt the encrypted energy or receive the desired energy [129].

V. MODERN ELECTRIC AND HYBRID VEHICLES

Internal combustion engine (ICE) vehicles have been involved in wide applications for over one hundred years, whereas these types of vehicles fail to meet the modern requirements, such as high fuel efficiency and low carbon emissions. Identified as one of the most viable solutions to the problems associated with ICE vehicles, EVs/HEVs have received significant attention in the past few decades. In this section, a few popular models with variation, namely Toyota Prius, Tesla Model S Plaid, and Porsche Taycan Turbo S are reviewed to highlight the development status of modern EVs/HEVs. It is just to illustrate different technologies with examples rather than a review of many EVs available in the market.

A. TOYOTA PRIUS XLE AWD-E

Toyota Prius is one of the most popular HEVs in the market, while it is famous for its excellent fuel efficiency. Fig. 14 shows the 2021 Prius XLE AWD-e that inherits the merits of the fourth-generation model of Toyota, and it employs all-wheel drive technology to improve driving performances.

TABLE 5. Specifications of Toyota Prius XLE AWD-e

Parameters	Prius XLE AWD-e [130]
Weight (kg)	1461
Powertrain	Hybrid transaxle
Mileage estimates (mpg city/ highway/combined)	51/47/49
Base price ($)	29,575
ENGINE	
Type	1.8-Liter, 4-Cyliner, DOHC
Max. power (hp @ rpm)	96 @ 5200
Max. torque (Nm @ rpm)	142 @ 3600
ELECTRIC MOTOR	
Type	PM AC motor
Power (hp)	71
Torque (Nm)	163
TRACTION BATTERY	
Type	Nickel-metal hydride (NiMH)
Voltage (V)	201.6

The fourth-generation Prius model has made collective innovations to deliver a 18% improvement in fuel efficiency, including a redesigned engine, an evolved hybrid transaxle, a compact Ni-MH battery, and a miniaturized power control unit [130].

As shown in Fig. 14(b), the most significant change in the fourth-generation Prius comes from its hybrid transaxle. Specifically, the drive motor and generator are located over multiple axles, and the planetary gear arrangement has been replaced with parallel gears. As a result, the mechanical loss is reduced by 20%, and the unit length is reduced by 47 mm. Another highlight is the high-performance engine can provide thermal efficiency of 40%, which is achieved by the strong airflow in combustion chambers, large-volume cooled exhaust gas recirculation (EGR), dual cooling system, and the newly designed water-cooling jacket. In addition, the use of low-loss components in the power control unit cuts losses by 20%, thus the unit size can be reduced by 33% accordingly. The detailed specifications of the 2021 Prius XLE AWD-e are summarized in Table 5. With the aforementioned improvements, the Prius XLE AWD-e can achieve an outstanding fuel efficiency of 49 mpg for combined working conditions.

B. TESLA MODEL S PLAID

Tesla has four series of EVs [131], namely Model X, Model Y, Model 3, and Model S. The first three EVs have drawn significant attention due to the desirable performances, while the Model S is widely regarded as the flagship of Tesla EVs. Fig. 15 shows the latest Tesla Model S Plaid, which has utilized the Tri-motor all-wheel drive (AWD) system. For existing AWD EVs, the complicated mechanical structures are adopted for power distribution from a single engine to all wheels, thus reducing the system efficiency. By contrast, for the Tri-motor AWD in Model S Plaid, one motor is placed in the front and the other two motors are arranged in the rear part of the EV. These three motors can be independently controlled to drive the front and rear wheels, and hence achieving fast acceleration and improved efficiency.

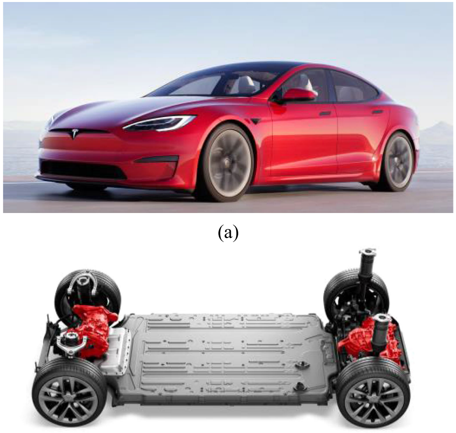

(a)

(b)

FIGURE 15. Tesla model S plaid [131]. (a) Overall view. (b) Tri-motor AWD system.

TABLE 6. Specifications of Model S Plaid and Porsche Taycan Turbo S

Parameters	Model S Plaid [131]	Taycan Turbo S [132]
Peak power (hp)	1020	751
Powertrain	Tri-motor AWD	AWD with two-speed transmission
Motor type	PM AC motor	
Torque (Nm)	1424	1050
Top speed (km/h)	322	260
Range (km)	637	340
Weight (kg)	2162	2370
Acceleration 0-100 km/h (s)	2.1	2.8
Supercharging max (kW)	250	262
Charging time (h)	6.5	9
Battery pack	Lithium-ion	
Battery capacity (kWh)	95	93.4
Battery useable (kWh)	90	83.7
Base price ($)	131,190	190,127

The specifications of Model S Plaid are listed in Table 6. It should be noted Model S Plaid can reach peak power of 1020 hp with top speed of 322 km/h. In addition, the speed acceleration from 0 to 100 km/h can be achieved within 2.1 seconds due to the promising powertrain. The driving range per charge can reach 637 km, which is much higher than the existing EV counterparts.

C. PORSCHE TAYCAN TURBO S

Porsche Taycan is the first attempt from Porsche in the EV market [132]. As the most powerful version of Porsche Taycan series, the Porsche Taycan Turbo S has been viewed as one of the best EVs in the world. Fig. 16 shows the Porsche Taycan Turbo S, which employs the two-speed transmission on the rear axle. This new powertrain is an unique technology from Porsche. There are two gears in the two-speed transmission system, i.e., one of the gears is utilized for initial speed acceleration and the other one is employed to keep the high power and efficiency at high speeds.

The specifications of Porsche Taycan Turbo S are listed in Table 6. It should be noted Porsche Taycan Turbo S can reach peak power of 751 hp with top speed of 260 km/h. In addition,

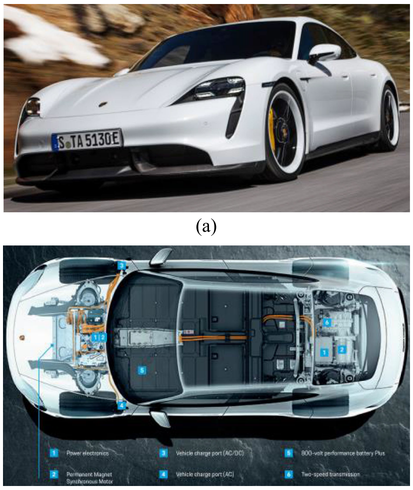

(a)

(b)

FIGURE 16. Porsche Taycan Turbo S [132]. (a) Overall view. (b) Drive unit.

the speed acceleration from 0 to 100 km/h can be achieved within 2.8 seconds. The driving range per charge can reach 340 km with approximately 9 h charging time.

VI. CONCLUSION

Due to the increasing concerns on energy crisis and energy utilization, development of EVs/HEVs has become a one-way train. There are plenty exciting technologies invented in the last few decades while an overview of emerging technologies can benefit many stakeholders. This paper aims to serve as a starting point for engineers, researchers and scholars who are keen to develop their interests in this area. In this paper, several key topics, namely electric machines, electrochemical energy sources, wireless charging infrastructures and latest EV/HEV models, are discussed in detail. This paper targets to provide the readers a blueprint for them to begin their own journey in the field.

REFERENCES

[1] M. Cheng, Z. Wang, and Y. Wong, *Encyclopedia of Automotive Engineering*. Wiley, 2015.

[2] Z. Wang, T. Ching, S. Huang, H. Wang, and T. Xu, "Challenges faced by electric vehicle motors and their solutions," *IEEE Access*, vol. 9, pp. 5228–5249, 2020.

[3] B. Dianati, S. Kahourzade, and A. Mahmoudi, "Optimization of axial-flux induction motors for the application of electric vehicles considering driving cycles," *IEEE Trans. Energy Convers.*, vol. 35, no. 3, pp. 1522–1533, Sep. 2020.

[4] N. V. Bharadwaj, P. Chandrasekhar, and M. Sivakumar , "Induction motor design analysis for electric vehicle application," in *AIP Conf. Proc.*, Oct. 2020, vol. 2269, no. 1, Art. no. 030038.

[5] D. Zechmair and K. Steidl, "Why the induction motor could be the better choice for your electric vehicle program," *World Electr. Veh. J.*, vol. 5, no. 2, pp. 546–549, 2012.

[6] M. Popescu, J. Goss, D. A. Staton, D. Hawkins, Y. C. Chong, and A. Boglietti, "Electrical vehicles-practical solutions for power traction motor systems," *IEEE Trans. Ind. Appl.*, vol. 54, no. 3, pp. 2751–2762, May/Jun. 2018.

[7] G. Sieklucki, "An investigation into the induction motor of Tesla model S vehicle," in *Proc. Int. Symp. Elect. Machines*, Andrychow, Poland, 2018, pp. 1–6.

[8] "Squirrel-cage rotor for an asynchronous machine, withdrawn patent," [Online]. Available: https://patents.google.com/patent/DE4308683A1/en

[9] R. Thomas, L. Garbuio, L. Gerbaud, and H. Chazal, "Modeling and design analysis of the Tesla model S induction motor," in *Proc. Int. Symp. Elect. Machines*, Gothenburg, Sweden, 2020, pp. 495–501.

[10] J. Mei, C. Lee, and J. Kirtley, "Design of axial flux induction motor with reduced back iron for electric vehicles," *IEEE Trans. Veh. Technol.*, vol. 69, no. 1, pp. 293–301, Jan. 2020.

[11] F. C. Mushid and D. G. Dorrell, "Review of axial flux induction motor for automotive applications," in *Proc. IEEE Workshop Elect. Machines Des., Control Diagnosis*, Nottingham, U.K., 2017, pp. 146–151.

[12] P. Y. Grachev, A. A. Bazarov, and A. S. Tabachinskiy, "Electrical and thermal processes of HEV induction machines taking into account stator winding form," in *Proc. Dyn. Syst., Mechanisms Machines (Dyn.)*, Omsk, Russia, 2017, pp. 1–6.

[13] F. Xie, K. Liang, W. Wu, W. Hong, and C. Qiu, "Multiple harmonic suppression method for induction motor based on hybrid morphological filters," *IEEE Access*, vol. 7, 2019, pp. 151618–151627.

[14] P. Han, M. Cheng, and Z. Chen, "Dual-electrical-port control of cascaded doubly-fed induction machine for EV/HEV applications," *IEEE Trans. Ind. Appl.*, vol. 53, no. 2, pp. 1390–1398, Mar./Apr. 2017.

[15] P. Han, M. Cheng, and Z. Chen, "Single-electrical-port control of cascaded doubly-fed induction machine for EV/HEV applications," *IEEE Trans. Power Electron.*, vol. 32, no. 9, pp. 7233–7243, Sep. 2017.

[16] J. D. Widmer, R. Martin, and M. Kimiabeigi, "Electric vehicle traction motors without rare earth magnets," *Sustain. Mater. Technol.*, vol. 3, pp. 7–13, Apr. 2015.

[17] T. Raminosoa *et al.*, "Sinusoidal reluctance machine with DC winding: An attractive non-permanent-magnet option," *IEEE Trans. Ind. Appl.*, vol. 52, no. 3, pp. 2129–2137, May 2016.

[18] Z. Q. Zhu, Z. Z. Wu, D. J. Evans, and W. Q. Chu, "A wound field switched flux machine with field and armature windings separately wound in double stators," *IEEE Trans. Energy Convers.*, vol. 30, no. 2, pp. 772–783, Jun. 2015.

[19] Y. Wang, S. Nuzzo, H. Zhang, W. Zhao, C. Gerada, and M. Galea, "Challenges and opportunities for wound field synchronous generators in future more electric aircraft," *IEEE Trans. Transp. Electrific.*, vol. 6, no. 4, pp. 1466–1477, Dec. 2020.

[20] G. Jawad, Q. Ali, T. A. Lipo, and B. Kwon, "Novel brushless wound rotor synchronous machine with zero-sequence third-harmonic field excitation," *IEEE Trans. Magn.*, vol. 52, no. 7, pp. 1–4, Jul. 2016.

[21] M. Michon, R. C. Holehouse, K. Atallah, and G. Johnstone, "Effect of rotor eccentricity in large synchronous machines," *IEEE Trans. Magn.*, vol. 50, no. 11, Nov. 2014, Art no. 8700404.

[22] O. Laldin, S. D. Sudhoff, and S. Pekarek, "An analytical design model for wound rotor synchronous machines," *IEEE Trans. Energy Convers.*, vol. 30, no. 4, pp. 1299–1309, Dec. 2015.

[23] J. K. Reed Ludois and K. Hanson, "Capacitive power transfer for rotor field current in synchronous machines," *IEEE Trans. Power Electron.*, vol. 27, no. 11, pp. 4638–4645, Nov. 2012.

[24] M. Ayub, A. Hussain, G. Jawad, and B. Kwon, "Brushless operation of a wound-field synchronous machine using a novel winding scheme," *IEEE Trans. Magn.*, vol. 55, no. 6, Jun. 2019, Art no. 8201104.

[25] F. Yao, Q. An, L. Sun, and T. A. Lipo, "Performance investigation of a brushless synchronous machine with additional harmonic field windings," *IEEE Trans. Ind. Electron.*, vol. 63, no. 11, pp. 6756–6766, Nov. 2016.

[26] F. Yao, Q. An, X. Gao, L. Sun, and T. A. Lipo, "Principle of operation and performance of a synchronous machine employing a new harmonic excitation scheme," *IEEE Trans. Ind. Appl.*, vol. 51, no. 5, pp. 3890–3898, Sep./Oct. 2015.

[27] A. Di Gioia *et al.*, "Design and demonstration of a wound field synchronous machine for electric vehicle traction with brushless capacitive field excitation," *IEEE Trans. Ind. Appl.*, vol. 54, no. 2, pp. 1390–1403, Mar./Apr. 2018.

[28] C. Pollock and M. Wallace, "The flux switching motor, a DC motor without magnets or brushes," in *Proc. Conf. Rec. IEEE IAS Annu. Meeting*, Phoenix, AZ, USA, 1999, vol. 3, pp. 1980–1987.

[29] J. T. Chen, Z. Q. Zhu, S. Iwasaki, and R. Deodhar, "Low cost flux-switching brushless AC machines," in *Proc. Conf. Veh. Pow. Prop.*, Lille, France, 2010, pp. 1–6.

[30] Z. Q. Zhu, Y. J. Zhou, J. T. Chen, and J. E. Green, "Investigation of nonoverlapping stator wound-field synchronous machines," *IEEE IEEE Trans. Energy Convers.*, vol. 30, no. 4, pp. 1420–1427, Dec. 2015.

[31] Z. Q. Zhu, Z. Z. Wu, D. J. Evans, and W. Q. Chu, "A wound field switched flux machine with field and armature windings separately wound in double stators," *IEEE Trans. Energy Convers.*, vol. 30, no. 2, pp. 772–783, Jun. 2015.

[32] Z. Z. Wu, Z. Q. Zhu, C. Wang, J. C. Mipo, S. Personnaz, and P. Farah, "Reduction of open-circuit DC-winding-induced voltage in wound field switched flux machines by skewing," *IEEE Trans. Ind. Electron.*, vol. 66, no. 3, pp. 1715–1726, Mar. 2019.

[33] Z. Wu, Z. Q. Zhu, C. Wang, J.-C. Mipo, S. Personnaz, and P. Farah, "Analysis and reduction of on-load DC winding induced voltage in wound field switched flux machines," *IEEE Trans. Ind. Electron.*, vol. 67, no. 4, pp. 2655–2666, Apr. 2020.

[34] Z. Wu *et al.*, "Analysis and suppression of induced voltage pulsation in DC winding of five-phase wound-field switched flux machines," *IEEE Trans. Energy Convers.*, vol. 34, no. 4, pp. 1890–1905, Dec. 2019.

[35] Z. Wu, Z. Q. Zhu, and C. Wang, "Reduction of On-load DC winding induced voltage in partitioned stator wound field switched flux machines by dual three-phase armature winding," *IEEE Trans. Ind. Electron*, to be published, doi: 10.1109/TIE.2021.3094482.

[36] X. Y. Sun, Z. Q. Zhu, S. Cai, L. Wang, F. R. Wei, and B. Shao, "Influence of stator slot and rotor pole number combination on field winding induced voltage ripple in hybrid excitation switched flux machine," *IEEE Trans. Energy Convers.*, vol. 36, no. 2, pp. 1245–1261, Jun. 2021.

[37] L. Yu, M. Zhang, Z. Zhang, and J. Bin, "Reduction of Field-winding-induced voltage in a doubly salient brushless DC generator with Stator-damper winding," *IEEE Trans. Ind. Electron.*, to be published, doi: 10.1109/TIE.2021.3105993.

[38] W. Zhang, W. Hua, Z. Wu, G. Zhao, Y. Wang, and W. Xia, "Analysis of DC winding induced voltage in wound-field flux-switching machine with air-gap field modulation principle," *IEEE Trans. Ind. Electron.*, to be published, doi: 10.1109/TIE.2021.3068684.

[39] J. Lin, N. Schofield, and A. Emadi, "External-rotor 6–10 switchedreluctance motor for an electric bicycle," *IEEE Trans. Transport. Electrific.*, vol. 1, no. 4, pp. 348–356, Dec. 2015.

[40] J. M. Miller, P. J. McCleer, and J. H. Lang, "Starter-alternator for hybrid electric vehicle: Comparison of induction and variable reluctance machines and drives," in *Proc. Conf. Rec. IEEE IAS Annu. Meeting*, St. Louis, MO, USA, 1998, vol. 1, pp. 513–523.

[41] P. A. Watterson *et al.*, "A switched-reluctance motor/generator for mild hybrid vehicles," in *Proc. Int. Conf. Elect. Mach. Syst.*, Wuhan, China, 2008, pp. 2808–2813.

[42] M. D. Hennen, M. Niessen, C. Heyers, H. J. Brauer, and R. W. De Doncker, "Development and control of an integrated and distributed inverter for a fault tolerant five-phase switched reluctance traction drive," in *Proc. Int. Power Electron. Motion Control Conf.*, Ohrid, Republic of Macedonia, 2010, pp. S11–S17.

[43] A. Chiba, "Torque density and efficiency improvements of a switched reluctance motor without rare-earth material for hybrid vehicles," *IEEE Trans. Ind. Appl.*, vol. 47, no. 3, pp. 1240–1246, May 2011.

[44] M. Takeno, A. Chiba, N. Hoshi, S. Ogasawara, M. Takemoto, and M. A. Rahman, "Test results and torque improvement of the 50-kW switched reluctance motor designed for hybrid electric vehicles," *IEEE Trans. Ind. Appl.*, vol. 48, no. 4, pp. 1327–1334, Jul. 2012.

[45] M. Zeraoulia, M. E. H. Benbouzid, and D. Diallo, "Electric motordrive selection issues for HEV propulsion systems: A comparativestudy," *IEEE Trans. Veh. Technol.*, vol. 55, no. 6, pp. 1756–1764, Nov. 2006.

[46] K. Kiyota and A. Chiba, "Design of switched reluctance motor competitive to 60-kW IPMSM in third-generation hybrid electric vehicle," *IEEE Trans. Ind. Appl.*, vol. 48, no. 6, pp. 2303–2309, Nov./Dec. 2012.

[47] E. Bostanci, M. Moallem, A. Parsapour, and B. Fahimi, "Opportunities and challenges of switched reluctance motor drives for electric propulsion: A comparative study," *IEEE Trans. Transp. Electrific.*, vol. 3, no. 1, pp. 58–75, Mar. 2017.

[48] T. Fukami, M. Momiyama, K. Shima, R. Hanaoka, and S. Takata, "Steady-state analysis of a dual-winding reluctance generator with a multiple-barrier rotor," *IEEE Trans. Energy Convers.*, vol. 23, no. 2, pp. 492–498, Jun. 2008.

[49] H. Kim and J. H. Lee, "Optimum design of ALA-SynRM for direct drive electric valve actuator," *IEEE Trans. Magn.*, vol. 53, no. 4, Apr. 2017, Art no. 8200804.

[50] A. A. Arkadan, A. A. Hanbali, and N. Al-Aawar, "Design optimization of ALA rotor SynRM drives using T-AI-EM environment," *IEEE Trans. Magn.*, vol. 43, no. 4, pp. 1645–1648, Apr. 2007.

[51] C. Babetto, G. Bacco, and N. Bianchi, "Synchronous reluctance machine optimization for high-speed applications," *IEEE Trans. Energy Convers.*, vol. 33, no. 3, pp. 1266–1273, Sep. 2018.

[52] G. Bacco, N. Bianchi, and H. Mahmoud, "A nonlinear analytical model for the rapid prediction of the torque of synchronous reluctance machines," *IEEE Trans. Energy Convers.*, vol. 33, no. 3, pp. 1539–1546, Sep. 2018.

[53] A. Accetta, M. Cirrincione, M. C. D. Piazza, G. L. Tona, M. Luna, and M. Pucci, "Analytical formulation of a maximum torque per ampere (MTPA) technique for synrms considering the magnetic saturation," *IEEE Trans. Ind. Appl.*, vol. 56, no. 4, pp. 3846–3854, Jul./Aug. 2020.

[54] M. H. Mohammadi, T. Rahman, R. C. P. Silva, B. Wang, K. Chang, and D. A. Lowther, "Effect of acoustic noise on optimal SynRM design regions," *IEEE Trans. Magn.*, vol. 54, no. 3, Mar. 2018, Art no. 8101304.

[55] M. Cheng, W. Hua, J. Zhang, and W. Zhao, "Overview of stator permanent magnet brushless machines," *IEEE Trans. Ind. Electron.*, vol. 58, no. 11, pp. 5087–5101, Nov. 2011.

[56] E. Hoang, A. Ben-Ahmed, and J. Lucidarme, "Switching flux permanent magnet polyphased synchronous machines," in *Proc. 7th Eur. Conf. Power Electron. Appl. EPE*, 1997, pp. 903–908.

[57] J. Chen, Z. Zhu, S. Iwasaki, and P. Deodhar, "A novel hybrid-excited switched-flux brushless ac machine for EV/HEV applications," *IEEE Trans. Veh. Techn.*, vol. 60, no. 4, pp. 1365–1373, May 2011.

[58] J. Chen, Z. Zhu, S. Iwasaki, and P. Deodhar, "Influence of slot opening on optimal stator and rotor pole combination and electromagnetic performance of switched-flux PM brushless AC machines," *IEEE Trans. Ind. Appl.*, vol. 47, no. 4, pp. 11681–11691, Jul./Aug. 2011.

[59] X. Zhu, Z. Shu, L. Quan, Z. Xiang, and X. Pan, "Design and multicondition comparison of two outer-rotor flux-switching permanent-magnet motors for in-wheel traction applications," *IEEE Trans. Ind. Electron.*, vol. 64, no. 8, pp. 6137–6148, Aug. 2017.

[60] G. Zhao and W. Hua, "Comparative study between a novel multi-tooth and a V-shaped flux-switching permanent magnet machines," *IEEE Trans. Magn.*, vol. 55, no. 7, Jul. 2019, Art. no. 8104908.

[61] E. Sulaiman, T. Kosaka, and N. Matsui, "High power density design of 6-slot–8-pole hybrid excitation flux switching machine for hybrid electric vehicles," *IEEE Trans. Magn.*, vol. 47, no. 10, pp. 4453–4456, Oct. 2011.

[62] W. Hua, M. Cheng, and G. Zhang, "A novel hybrid excitation flux-switching motor for hybrid vehicles," *IEEE Trans. Magn.*, vol. 45, no. 10, pp. 4728–4731, Oct. 2009.

[63] G. Zhang, W. Hua, M. Cheng, J. Liao, K. Wang, and J. Zhang, "Investigation of an improved hybrid-excitation flux-switching brushless machine for HEV/EV applications," *IEEE Trans. Ind. Appl.*, vol. 51, no. 5, pp. 3791–3799, Sep./Oct. 2015.

[64] Christopher H. T. Lee, James L. Kirtley, and M. Angle, "A partitioned-stator flux-switching permanent-magnet machine with mechanical flux adjusters for hybrid electric vehicles," *IEEE Trans. Magn.*, vol. 53, no. 11, May 2017, Art. no. 3000807.

[65] W. Ullah, F. Khan, and M. Umair, "Design and optimization of segmented PM consequent pole hybrid excited flux switching machine for EV/HEV application," *CES Trans. Elect. Machines Syst.*, vol. 4, no. 3, pp. 206–214, Sep. 2020.

[66] W. Hua, X. Yin, G. Zhang, and M. Cheng, "Analysis of two novel five-phase hybrid-excitation flux-switching machines for electric vehicles," *IEEE Trans. Magn.*, vol. 50, no. 11, Nov. 2011, Art. no. 8700305.

[67] Y. Maeda, T. Kosaka, and N. Matsui, "Design study on hybrid excitation flux switching motor with permanent magnet placed at middle of field coil slot for HEV drives," in *Proc. Int. Conf. Elect. Machines*, Lausanne, Switzerland, 2016, pp. 2522–2528.

[68] W. Hua, M. Cheng, and Z. Q. Zhu, "Analysis and optimization of back EMF waveform of a flux-switching permanent magnet motor," *IEEE Trans. Energy Conver.*, vol. 3, no. 23, pp. 727–733, Sep. 2008.

[69] X. Zhu, W. Hua, and W. Wang, "Analysis of back-EMF in flux-reversal permanent magnet machines by air gap field modulation theory," *IEEE Trans. Ind. Electron.*, vol. 5, no. 66, pp. 3344–3355, May 2019.

[70] M. Cheng, K. T. Chau, and C. C. Chan, "Static characteristics of a new doubly salient permanent magnet motor," *IEEE Trans. Energy Conver.*, vol. 1, no. 16, pp. 20–25, Mar. 2001.

[71] D. J. Rhodes, "Assessment of Vernier motor design using generalised machine concepts," *IEEE Trans. Power App. Syst.*, vol. 4, no. 96, pp. 1346–1352, Jul. 1977.
[72] M. Cheng, H. Wen, and P. Han, "Analysis of airgap field modulation principle of simple salient poles," *IEEE Trans. Ind. Electron.*, vol. 4, no. 66, pp. 2628–2638, Apr. 2019.
[73] Z. Z. Wu and Z. Q. Zhu, "Analysis of air-gap field modulation and magnetic gearing effects in switched flux permanent magnet machines," *IEEE Trans. Magn.*, vol. 5, no. 51, pp. 1–12, May 2015.
[74] P. Wang, W. Hua, and G. Zhang, "Principle of flux-switching PM machine by magnetic field modulation theory part II: Electromagnetic torque generation," *IEEE Trans. Ind. Electron.*, vol. 69, no. 3, pp. 2437–2446, Mar. 2022.
[75] M. Cheng, P. Han, and W. Hua, "General airgap field modulation theory for electrical machines," *IEEE Trans. Ind. Electron.*, vol. 8, no. 64, pp. 6063–6074, Aug. 2017.
[76] L. Jian, K. T. Chau, and Y. Gong, "Comparison of coaxial magnetic gears with different topologies," *IEEE Trans. Magn.*, vol. 10, no. 45, pp. 4526–4529, Oct. 2009.
[77] Y. Liao, F. Liang, and T. A. Lipo, "A novel permanent magnet motor with doubly salient structure," *IEEE Trans. Ind. Appl.*, vol. 5, no. 31, pp. 1069–1078, Sep./Oct. 1995.
[78] T. H. Kim and J. Lee, "A study of the design for the flux reversal machine," *IEEE Trans. Magn.*, vol. 4, no. 40, pp. 2053–2055, Jul. 2004.
[79] J. Li and K. T. Chau, "Performance and cost comparison of permanent-magnet vernier machines," *IEEE Trans. Appl. Supercon.*, vol. 3, no. 22, pp. 5202304–5202304, Jun. 2012.
[80] R. Ishikawa, K. Sato, and S. Shimomura, "Design of in-wheel permanent magnet vernier machine to reduce the armature current density," in *Proc. Int. Conf. Elect. Machines Syst.*, Busan, Korea, 2013, pp. 459–464.
[81] J. Li, K. T. Chau, and W. Li, "Harmonic analysis and comparison of permanent magnet vernier and magnetic-geared machines," *IEEE Trans. Magn.*, vol. 10, no. 47, pp. 3649–3652, Oct. 2011.
[82] S. L. Ho, S. Niu, and W. N. Fu, "Design and comparison of vernier permanent magnet machines," *IEEE Trans. Magn.*, vol. 10, no. 47, pp. 3280–3283, Oct. 2011.
[83] Y. Zhang, H. Lin, and S. Fang, "Air-gap flux density characteristics comparison and analysis of permanent magnet vernier machines with different rotor topologies," *IEEE Trans. Appl. Supercon.*, vol. 4, no. 26, pp. 1–5, Jun. 2016.
[84] Z. Yang, F. Shang, I. P. Brown, and M. Krishnamurthy, "Comparative study of interior permanent magnet, induction, and switched reluctance motor drives for EV and HEV applications," *IEEE Trans. Transp. Electr.*, vol. 1, no. 3, pp. 245–254, Oct. 2015.
[85] I López, E Ibarra, and A Matallana *et al.*, "Next generation electric drives for HEV/EV propulsion systems: Technology, trends and challenges," *Renewable Sustain. Energy Rev.*, vol. 114, 2019, Art no. 109336.
[86] J. Dong, Y. Huang, L. Jin, and H. Lin, "Comparative study of surface-mounted and interior permanent-magnet motors for high-speed applications," *IEEE Trans. Appl. Supercon.*, vol. 26, no. 4, Jun. 2016, Art no. 5200304.
[87] E. Agamloh, A. von Jouanne, and A. Yokochi, "An overview of electric machine trends in modern electric vehicles," *Machines*, vol. 8, no. 2, Apr. 2020, Art. no. 20.
[88] T. Tomioka and K. Akatsu, "Study of High-speed SRM with amorphous steel sheet for eV," in *Proc. 22nd Int. Conf. Elect. Machines Syst.*, Chiba, Japan, 2019, pp. 1–6.
[89] E. W. Fairall, B. Bilgin, and A. Emadi, "State-of-the-art high-speed switched reluctance machines," in *Proc. IEEE Int. Electric Machines Drives Conf.*, Coeur d'Alene, ID, USA, May 2015, pp. 1621–1627.
[90] N. Uzhegov, J. Barta, J. Kurfürst, C. Ondrusek, and J. Pyrhönen, "Comparison of high-speed electrical motors for a turbo circulator application," *IEEE Trans. Ind. Appli.*, vol. 53, no. 5, pp. 4308–4317, Sep./Oct. 2017.
[91] B. Wang, J. Wang, A. Griffo, and B. Sen, "Stator turn fault detection by second harmonic in instantaneous power for a triple-redundant fault-tolerant PM drive," *IEEE Trans. Ind. Electron.*, vol. 65, no. 9, pp. 7279–7289, Sep. 2018.
[92] J. Skrabak, P. Rafajdus, P. Makys, and R. Bastovansky, "Design of high speed reluctance synchronous motor for automotive purposes," in *Proc. Int. Conf. Expo. Elect. Power Eng.*, Iasi, Romania, 2018, pp. 0427–0432.
[93] J. Lee, D. Jung, J. Lim, K. Lee, and J. Lee, "A study on the synchronous reluctance motor design for high torque by using RSM," *IEEE Trans. Magn.*, vol. 54, no. 3, Mar. 2018, Art. no. 8103005.
[94] E. Carraro, M. Degano, M. Morandin, and N. Bianchi, "PM synchronous machine comparison for light electric vehicles," in *Proc. IEEE Int. Electric Veh. Conf.*, Florence, Italy, 2014, pp. 1–8.
[95] B. Ozpineci, Oak Ridge National Laboratory Annual Progress Report for the Power Electronics and Electric Machinery Program, Oak Ridge Nat. Lab., Oak Ridge, TN, USA, 2016.
[96] A. Di Gerlando, G. M. Foglia, M. F. Iacchetti, and R. Perini, "Parasitic currents in stray paths of some topologies of YASA AFPM machines: Trend with machine size," *IEEE Trans. Ind. Electron.*, vol. 63, no. 5, pp. 2746–2756, May 2016.
[97] E. Chang, "High-speed hybrid reluctance motor with anisotropic materials," *General Motors*, Jun. 2021. [Online]. Available: https://www.energy.gov/eere/vehicles/articles/high-speed-hybrid-reluctance-motor-anisotropic-materials
[98] D. Gerada, H. Zhang, Z. Xu, G. L. Calzo, and C. Gerada, "Electrical machine type selection for high speed supercharger automotive applications," in *Proc. 19th Int. Conf. Elect. Machines Syst.*, Chiba, Japan, 2016, pp. 1–6.
[99] A. Vagati, G. Pellegrino, and P. Guglielmi, "Comparison between SPM and IPM motor drives for EV application," in *Proc. XIX Int. Conf. Elect. Machines*, Rome, Italy, 2010, pp. 1–6.
[100] H. Q. Li, G. M. Weng, C. Y. V. Li, and K. Y. Chan, "Three electrolyte high voltage acid-alkaline hybrid rechargeable battery," *Electrochimica Acta*, vol. 56, no. 25, pp. 9420–9425, 2011.
[101] T. Reddy, *Linden's Handbook of Batteries*. New York, NY, USA: McGraw-Hill Education, 2011.
[102] S. Revankar and P. Majumdar, *Fuel Cells: Principles Design and Analysis*. Boca Raton, FL, USA: CRC Press, 2014.
[103] S. Whittingham, "History, evolution, and future status of energy storage," *Proc. IEEE*, vol. 100, pp. 1518–1534, May 2012.
[104] A. F. Burke, "Batteries and ultracapacitors for electric, hybrid, and fuel cell vehicles," *Proc. IEEE*, vol. 95, no. 4, pp. 806–820, Apr. 2007.
[105] R. P. Desphande, *Ultracapacitors*. New York, NY, USA: McGraw-Hill Education, 2015.
[106] C. Jiang, D. E. Gaona, Y. Shen, H. Zhao, K. Chau, and T. Long, "Low frequency medium power capacitor-free self-resonant wireless power transfer," *IEEE Trans. Ind. Electron.*, vol. 68, no. 11, pp. 10521–10533, Nov. 2021.
[107] C. Jiang, K. T. Chau, W. Liu, C. Liu, W. Han, and W. H. Lam, "An LCC-compensated multiple-frequency wireless motor system," *IEEE Trans. Ind. Inform.*, vol. 15, no. 11, pp. 6023–6034, Nov. 2019.
[108] C. Jiang, K. Chau, Y. Y. Leung, C. Liu, C. H. Lee, and W. Han, "Design and analysis of wireless ballastless fluorescent lighting," *IEEE Trans. Ind. Electron.*, vol. 66, no. 5, pp. 4065–4074, May 2019.
[109] C. Jiang, K. Chau, C. Liu, C. H. Lee, W. Han, and W. Liu, "Move-and-charge system for automatic guided vehicles," *IEEE Trans. Magn.*, vol. 54, no. 11, Nov. 2018, Art. no. 8600105.
[110] J. Pries, V. P. N. Galigekere, O. C. Onar, and G.-J. Su, "A 50-kW three-phase wireless power transfer system using bipolar windings and series resonant networks for rotating magnetic fields," *IEEE Trans. Power Electron.*, vol. 35, no. 5, pp. 4500–4517, May 2020.
[111] S. Y. R. Hui, W. Zhong, and C. K. Lee, "A critical review of recent progress in mid-range wireless power transfer," *IEEE Trans. Power Electron.*, vol. 29, no. 9, pp. 4500–4511, Sep. 2014.
[112] D. E. Gaona-Erazo, C. Jiang, and T. Long, "Highly efficient 11.1 kW wireless power transfer utilizing nanocrystalline ribbon cores," *IEEE Trans. Power Electron.*, vol. 36, no. 9, pp. 9955–9969, Sep. 2021.
[113] C. Jiang, K. T. Chau, C. Liu, and C. H. T. Lee, "An overview of resonant circuits for wireless power transfer," *Energies*, vol. 10, no. 7, pp. 894:1–89420, Jun. 2017.
[114] K. T. Chau, C. Jiang, W. Han, and C. H. T. Lee, "State-of-the-art electromagnetics research in electric and hybrid vehicles," *Prog. Electromagnetics Res.*, vol. 159, pp. 139–157, Oct. 2017.
[115] A. Zaheer, H. Hao, G. A. Covic, and D. Kacprzak, "Investigation of multiple decoupled coil primary pad topologies in lumped IPT systems for interoperable electric vehicle charging," *IEEE Trans. Power Electron.*, vol. 30, no. 4, pp. 1937–1955, Apr. 2015.
[116] Y. Liu, U. K. Madawala, R. Mai, and Z. He, "Zero-phase-angle controlled bidirectional wireless EV charging systems for large

coil misalignments," *IEEE Trans. Power Electron.*, vol. 35, no. 5, pp. 5343–5353, May 2020.
[117] M. Bojarski, K. K. Kutty, D. Czarkowski, and F. De Leon, "Multiphase resonant inverters for bidirectional wireless power transfer," in *Proc. IEEE Int. Electric Veh. Conf.*, Florence, Italy, 2014, pp. 1–7.
[118] Z. Yan, Z. Xiang, L. Wu, and B. Wang, "Study of wireless power and information transmission technology based on the triangular current waveform," *IEEE Trans. Power Electron.*, vol. 33, no. 2, pp. 1368–1377, Feb. 2018.
[119] C. Jiang, K.-T. Chau, W. Han, and W. Liu, "Development of multi-layer rectangular coils for multiple-receiver multiple-frequency wireless power transfer," *Prog. Electromagn. Res.*, vol. 163, pp. 15–24, 2018.
[120] M. G. S. Pearce, G. A. Covic, and J. T. Boys, "Robust ferrite-less double d topology for roadway IPT applications," *IEEE Trans. Power Electron.*, vol. 34, no. 7, pp. 6062–6075, Jul. 2019.
[121] J. T. Boys and G. A. Covic, "The inductive power transfer story at the University of Auckland," *IEEE Circuits Syst. Mag.*, vol. 15, no. 2, pp. 6–27, Apr./Jun. 2015.
[122] A. Zaheer, H. Hao, G. A. Covic, and D. Kacprzak, "Investigation of multiple decoupled coil primary pad topologies in lumped IPT systems for interoperable electric vehicle charging," *IEEE Trans. Power Electron.*, vol. 30, no. 4, pp. 1937–1955, Apr. 2015.
[123] C. C. Mi, G. Buja, S. Y. Choi, and C. T. Rim, "Modern advances in wireless power transfer systems for roadway powered electric vehicles," *IEEE Trans. Ind. Electron.*, vol. 63, no. 10, pp. 6533–6545, Oct. 2016.
[124] S. Y. Choi, B. W. Gu, S. Y. Jeong, and C. T. Rim, "Advances in wireless power transfer systems for roadway-powered electric vehicles," *IEEE J. Emerg. Sel. Topics Power Electron.*, vol. 3, no. 1, pp. 18–36, Mar. 2015.
[125] J. Huh, S. W. Lee, W. Y. Lee, G. H. Cho, and C. T. Rim, "Narrow-width inductive power transfer system for online electrical vehicles," *IEEE Trans. Power Electron.*, vol. 26, no. 12, pp. 3666–3679, Dec. 2011.
[126] W. Han, K. T. Chau, Z. Zhang, and C. Jiang, "Single-source multiple-coil homogeneous induction heating," *IEEE Trans. Magn.*, vol. 53, no. 11, Jun. 2017, Art. no. 7207706.
[127] C. Jiang, K.-T. Chau, C. H. T. Lee, W. Han, W. Liu, and W.-H. Lam, "Development of multiple-frequency wireless coordinative motor drives," *Prog. Electromagn. Res. C*, vol. 91, pp. 143–156, 2019.
[128] W. Liu, K. Chau, C. H. T. Lee, C. Jiang, W. Han, and W. Lam, "Wireless energy-on-demand using magnetic quasi-resonant coupling," *IEEE Trans. Power Electron.*, vol. 35, no. 9, pp. 9057–9069, Sep. 2020.
[129] Z. Zhang, K. T. Chau, C. Qiu, and C. Liu, "Energy encryption for wireless power transfer," *IEEE Trans. Power Electron.*, vol. 30, no. 9, pp. 5237–5246, Sep. 2015.
[130] Toyota Co. Ltd., "Prius," 2022, [Online]. Available: https://www.toyota.com/prius/
[131] Tesla Co. Ltd., "Tesla Model S plaid," 2021, [Online]. Available: http://www.tesla.com/models
[132] Porsche Co. Ltd., "Porsche Taycan Turbo S," 2021, [Online]. Available: https://www.porsche.com/Singapore/en/models/taycan/taycan-models/taycan-turbo-s/

CHRISTOPHER H. T. LEE (Senior Member, IEEE) received the B.Eng. (first-class Hons.) and Ph.D. degrees in electrical engineering from the Department of Electrical and Electronic Engineering, The University of Hong Kong, Hong Kong. He is currently an Assistant Professor with Nanyang Technological University, Singapore, and Honorary Assistant Professor with The University of Hong Kong. He was a Postdoctoral Fellow and then a Visiting Assistant Professor with the Massachusetts Institute of Technology, Cambridge, MA, USA. He has authored or coauthored one book, three books chapters, and more than 100 referred papers in his research field, which include electric machines and drives, renewable energies, and electromechanical propulsion technologies. He is an Associate Editor for the IEEE TRANSACTIONS ON INDUSTRIAL ELECTRONICS, IEEE TRANSACTIONS ON ENERGY CONVERSION, IEEE ACCESS, and *IET Renewable Power Generation*. He is a Chartered Engineer in Hong Kong. Dr. Lee was the recipient of many awards, including the NRF Fellowship, Nanyang Assistant Professorship, Li Ka Shing Prize (the best Ph.D. thesis prize) and Croucher Foundation Fellowship.

WEI HUA (Senior Member, IEEE) received the B.Sc. and Ph.D. degrees in electrical engineering from Southeast University, Nanjing, China, in 2001 and 2007, respectively. From 2004 to 2005, he was with the Department of Electronics and Electrical Engineering, The University of Sheffield, Sheffield, U.K., as a Joint-Supervised Ph.D. Student. Since 2007, he has been with Southeast University, where he is currently a Chief Professor and a Distinguished Professor of Jiangsu Province. In 2010, he was also with the Yancheng Institute of New Energy Vehicles, Southeast University. He has coauthored more than 150 technical papers. He holds 50 patents in his areas of interest. His teaching and research interests include design, analysis, and control of electrical machines, especially for PM brushless machines and switching reluctance machines.

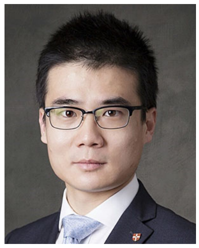

TENG LONG (Member, IEEE) received the B.Eng. degree from the Huazhong University of Science and Technology, Wuhan, China, the B.Eng. (first-class Hons.) degree from the University of Birmingham, Birmingham, U.K. in 2009, and the Ph.D. degree from the University of Cambridge, Cambridge, U.K. in 2013. Until 2016, he was a Power Electronics Engineer with General Electric (GE) Power Conversion Business, Rugby, U.K. He is currently an Associate Professor with the University of Cambridge. His research interests include power electronics, electrical machines, and machine drives. Dr. Long is a Chartered Engineer (CEng) registered with the Engineering Council in the U.K.

CHAOQIANG JIANG (Member, IEEE) received the B.Eng. and M.Eng. degrees (first-class Hons.) in electrical engineering and automation from Wuhan University, Wuhan, China, in 2012 and 2015, respectively, and the Ph.D. degree in electrical and electronic engineering from The University of Hong Kong, Hong Kong, in 2019. He is currently an Assistant Professor with the Department of Electrical Engineering, and a Faculty Member with the State Key Laboratory of Terahertz and Millimeter Waves, City University of Hong Kong, Hong Kong. From 2019 to 2021, he was a Postdoctoral Research Associate with the University of Cambridge, Cambridge, U.K. Since 2021, he has been affiliated with the Clare Hall, University of Cambridge. In 2019, he was a Visiting Researcher with Nanyang Technological University, Singapore. His research interests include power electronics, wireless power transfer techniques, electric machines and drives, and electric vehicle (EV) technologies. Dr. Jiang is currently an Associate Editor for the *IET Renewable Power Generation*, the Guest Editor of the IEEE OPEN JOURNAL OF VEHICULAR TECHNOLOGY, and the Guest Editor of the *Energies*. He was rewarded with the Winner, CAPE Acorn Blue Sky Research Award at the University of Cambridge, and First Prize in the Interdisciplinary Research Competition at the University of Hong Kong.

LAKSHMI VARAHA IYER (Senior Member, IEEE) received the B.Tech. degree in electronics and communication engineering from SASTRA University, Thanjavur, India, and the M.A.Sc. and Ph.D. degrees in electrical and computer engineering from the University of Windsor, Windsor, ON, Canada. He is currently an Engineering Manager with Magna International's Corporate R&D Division. Since 2008, he has been innovating in the area of electric machines and power electronics for electrified automotive and renewable energy applications, in the roles of an Intern with Infineon Technologies, a Graduate Student, Research Associate, Research Scientist and Industry Liaison Officer, Adjunct Professor with the University of Windsor, a Technical Specialist and Engineering Manager with Magna International Inc. He has authored or coauthored more than 60 peer-reviewed papers in international conferences and journals has authored or coauthored more than 20 patents. He was the recipient of the 2017 Governor General's Gold Medal in Canada and one among North America's "30 under 30" honored by Society of Manufacturing Engineers in 2018. He is an Associate Editor for the IEEE TRANSACTIONS ON POWER ELECTRONICS.